Submitted to ADVANCED MATERIALS

DOI: 10.1002//adma.((please add manuscript number))

Radiation Hardness and Self-Healing of Perovskite Solar Cells

By *F. Lang*, N. H. Nickel, J. Bundesmann, S. Seidel, A. Denker, S. Albrecht, V. V. Brus, J. Rappich, B. Rech, G. Landi, and H. C. Neitzert*

[*] F. Lang, Prof. Dr. N. H. Nickel, Dr. S. Albrecht, Dr. V. V. Brus, Dr. J. Rappich, Prof. Dr. B. Rech
Helmholtz-Zentrum Berlin für Materialien und Energie GmbH, Institut für Silizium Photovoltaik, Kekuléstr. 5, 12489 Berlin, Germany.
E-mail: felix.lang@helmholtz-berlin.de

J. Bundesmann, S. Seidel, Dr. A. Denker
Helmholtz-Zentrum Berlin für Materialien und Energie GmbH, Protons for Therapy, Hahn-Meitner Platz 1, 14109 Berlin, Germany

Dr. G. Landi, Prof. Dr. H. C. Neitzert
Dept. of Industrial Engineering (DIIn), Salerno University, Via Giovanni Paolo II 132, 84084 Fisciano (SA), Italy

Keywords: perovskite solar cells, radiation hardness, proton irradiation, degradation, self-healing

Thin-film tandem solar cells, comprising of a perovskite top junction and a radiation hard CIGS bottom junction are attractive for space applications since they can be thin, lightweight, flexible, and efficient. The ability to withstand the harsh radiation environment in space, consisting mainly of high-energy protons is demonstrated. In-situ measurements of the *J*-V characteristics during proton irradiation with an energy of 68 MeV reveal the stability of these novel organic-inorganic perovskites. The investigated $CH_3NH_3PbI_3$ based perovskite solar cells possess a negligible degradation for doses of up to 10^{12} p cm^{-2}. The observed degradation at very high doses is dominated by coloring of the glass substrate. Taking this effect and the photo-degradation into account the proton-induced absorber degradation shows a change of J_{SC} by only 15 % at a proton dose of 10^{13} p cm^{-2}. The Voc does not degrade. In addition to the superior radiation hardness, $CH_3NH_3PbI_3$ exhibits a self-healing mechanism when the proton irradiation is terminated. This process effectively mitigates radiation induced

localized defects. The photocurrent and the photovoltaic performance of the perovskite therefore recover with time.

1. Introduction

Solar cells based on hybrid perovskites, such as methyl ammonium lead iodide ($CH_3NH_3PbI_3$), showed already excellent device performances with efficiencies exceeding 20 %[1] after an impressive short research and development time.[1,2] Band-gap tuning over a wide energy range [3–5] makes this class of materials interesting for multi-junction solar cells with ultra-high efficiencies. Tandem solar-cells combining perovskites with Si[5–12], $Cu(In,Ga)Se_2$[9,13], and $Cu_2ZnSn(S,Se)_4$[14] have been reported. Such high power multi-junction solar cells are needed for spaceships and satellites in outer space, where efficiency, size, and weight represent important factors. On the other hand, ionizing radiation, mainly helium (He) and protons (p), originating from either galactic cosmic radiation or solar flares is known to affect electronic devices by defect creation. [15] The particle flux varies between 10^3 and 10^8 particles cm^{-2} s^{-1} depending on exposition and distance from earth.[16–19] A dose of 10^{13} particles cm^{-2}, as used later in our study, therefore accumulates over 30 years or 1 day. The ionizing radiation has a tremendous effect on the power conversion efficiency of silicon, InGaP, GaAs, and InP solar cells that are commonly used in space. [20] For example, the Equator-S Mission, equipped with an GaAs/Ge solar cell reported a reduction in efficiency of around 10 % after 30 days in the low earth orbit.[21] Interestingly, one of the most radiation resistant solar-cell absorber materials, namely, copper indium gallium di-selenide (CIGS)[20] is rarely used due to its moderate power-conversion efficiency.[22] A thin-film tandem solar cell comprising of a CIGS bottom- and a perovskite top junction seems to be an ideal candidate to overcome this limitation. In principle, the combination should allow a new generation of efficient, lightweight, thin, and flexible solar-cell arrays for space applications. Solar-cell array foils that self-enfold once launched into orbit are imaginable.[23] Moreover

radiation resistant semiconductors based on hybrid perovskites might enable novel sensors and transistors that are capable to work within the environment of damaged and running nuclear power plants.

However, before such revolutionary designs will be implemented, the radiation resistance of these organic-inorganic perovskites has to be demonstrated. Therefore, we present a study on the radiation hardness of $CH_3NH_3PbI_3$ using 68 MeV proton irradiation. *In-situ* measurements revealed a superior radiation resistance in comparison to a commercially available crystalline silicon (c-Si) photo-diode. In light of the reported instabilities of perovskite solar cells, the observed radiation resistance is remarkable. [24]

2. Results and Discussion

Proton-induced defect creation occurs due to ionization and lattice displacement effects. In addition, proton irradiation can also stimulate nuclear reactions due to proton capture of atoms. Typically, the newly generated nuclei are radioactive. Therefore, after the radiation experiments the samples must remain in the radiation safety controlled area delaying device characterization of the sensitive perovskites. In order to investigate the radiation hardness of the hybrid perovskite $CH_3NH_3PbI_3$, we decided to track the development the photovoltaic parameters *in-situ* under illumination during irradiation with protons. An automated system therefore recorded the *J*-V curves of 4 devices simultaneously every 30 seconds. Two of these devices were exposed to proton irradiation, while the two others serve as reference. Proper encapsulation further allowed to take additional measurements after the radioactivity dropped to a bearable level.

2.1. Solar Cell Performance

Typical perovskite solar cells based on TiO_2 and spiro-OMeTAD show pronounced hysteresis effects. [25–27] This would complicate the correct analysis of the *in-situ* measurements during proton irradiation. Therefore, we chose the inverted structure with a layer sequence of glass/ITO/PEDOT:PSS/$CH_3NH_3PbI_3$/PCBM/BCP/Ag. This structure has the advantage that a hysteresis of the *J*–V characteristics is negligible. [26] Fig. 1(b) shows a simplified sketch of the used device structure and a cross-sectional scanning electron microscopy (SEM) micrograph is depicted in Fig 1(a). The film homogeneity is controlled by using a mixture of the solvents γ-butryolactone (GBL) / dimethyl sulfoxide (DMSO) and by a toluene dripping in a late spin coating stage. [28] Details on the device preparation are given in the experimental section.

Figure 1(d) shows the current-voltage characteristics of fabricated solar cells under AM 1.5G illumination. Due to the used inverted structure a hysteresis in the *J*-V curves is negligible. The power conversion efficiency derived from the *J*-V curve amounted to η = 12.0 % (see Fig. 1(d)). The result is corroborated using an maximum power point (MPP) tracking algorithm, as shown in the inset of Fig. 1(d)). The obtained stabilized value of η = 12.1 % obtained after 400 s, matched the *J*-V measurement perfectly. Fill factor, open circuit voltage and short circuit current amounted to FF = 71 %, V_{OC} = 0.95 V and J_{SC} = 17.9 mA/cm^2. Due to the stabilized performance & the absence of hysteresis effects, the solar cells employed in this study are well suited to investigate degradation effects related to the absorber radiation hardness. The external (EQE) and internal quantum efficiencies (IQE) are depicted in Fig. 1(e). The integrated short circuit current amounts to 17.4 mAcm^{-2} and matches the value obtained under AM1.5 illumination.

2.2 Radiation Hardness under Proton Irradiation

Ionizing radiation in space is dominated by high energy protons in the MeV range[29,30]. In particular, protons with energies close to 1 MeV have a high stopping cross-section and therefore, can cause severe damage to electronic devices and solar cells.[31] On the other hand, an effective radiation guard requires only a view millimeters of shielding. Thus, for our study we have chosen a proton energy of 68 MeV that still causes considerable damage while having a projected range of several centimeters. This ensures homogeneous defect creation throughout the entire perovskite absorber. The proton energy-loss is shown in Fig. 1(c) as a function of the target depth. The data were derived from a SRIM calculation.[32]

Three identical perovskite solar cells were exposed to proton irradiation with a total proton dose of $\phi = 1.02\times10^{13}$ p cm^{-2}. The experiments were performed at the cyclotron facility of the Helmholtz-Zentrum Berlin. [33,34] The proton flux was kept constant around $\varphi = 1.68\times10^{9}$ p cm^{-2} s^{-1}. The total dose of 1.02×10^{13} p cm^{-2} therefore was accumulated after 101 min. Fig. 2 shows the degradation the photovoltaic parameters of two irradiated devices, red open and closed symbols, as a function of the proton dose, ϕ. Two simultaneously measured, but not irradiated devices serve as reference, black open and closed diamonds.

Fig. 2(a) shows the evolution of J_{SC}, derived from in-situ measurements taken every 30 seconds. The data is normalized to $\phi = 0$. Upon proton irradiation J_{SC} of the solar cells decreases (red symbols). This is due to the generation of localized defects. It is important to note that the perovskite solar cells do not exhibit any degradation for a proton dose of $\phi \leq 2\times10^{11}$ p cm^{-2}. Only at higher proton doses a decrease of J_{SC} is observed with a reduction of around 10 % and 60 % for $\phi = 10^{12}$ p cm^{-2} and 10^{13} p cm^{-2}, respectively. On the other hand, the impact of proton-irradiation experiments on the short-circuit current of a commercially available c-Si photo diode shows pronounced degradation due to defect creation even for a low proton dose. We therefore tracked the *J*sc only, allowing superior time and thus dose resolution, as compared to complete measurements of the *J*-V curve. A 20 % decrease of the

photo current is observed for a proton dose of only $\phi = 10^{11}$ p cm^{-2} (blue curve in Fig. 2(a)). This is in good agreement with previous reports for c-Si solar cells.[35] The data shown in Fig. 2 (a) clearly demonstrate that perovskite solar cells are significantly less affected by proton radiation than c-Si devices.

On the other hand also the non irradiated perovskite reference device degrades significantly over time during illumination (Fig 2(a) black open and closed diamonds). Since *in-situ* measurements of the solar cells were performed during proton irradiation the photo-induced degradation of the devices has to be taken into account. For a proton dose of $\phi = 10^{12}$ p cm^{-2} and $\phi = 10^{13}$ p cm^{-2} a decrease of J_{SC} of about 3.8 % and 15 %, respectively, is observed. The perovskite layers therefore can withstand proton doses as high as 10^{12} p cm^{-2} before degradation commences. This exceeds the proton dose at which c-Si begins to degrade by almost 3 orders of magnitude. Hence, we have experimentally demonstrated that the perovskite layers are radiation hard making them a desirable material in solar cells for space applications.

In case of c-Si, an additional degradation of the V_{OC} of around 11 % at a dose of $\phi = 5\times10^{12}$ p cm^{-2} is reported in literature. [35] For perovskite no effect on V_{OC} and FF is noticeable for doses up to $\phi = 10^{13}$ p cm^{-2}, as shown in Fig 2(b) and (d). The power conversion efficiency of the perovskite solar cell therefore follows the degradation in J_{SC} only, Fig. 2(c).

The series (R_S) and parallel (R_P) resistance can be estimated from the slope of the *J*-V curves according to equation 1.

$$R_P = -\left(\frac{dU}{dJ}\right)_{V_{OC}},\ R_S = -\left(\frac{dU}{dJ}\right)_{Jsc} \quad (1)$$

The evolution of R_S and R_P might allow some insight into the degradation mechanisms. However the observed absolute changes are rather small. In fact an influence on the FF is imperceptible. Fig.2 (e) and (f) show the relative evolution of R_P and R_S upon irradiation. R_P

increases for both the reference and the irradiated device. Following the theory by Dittrich et al. we might assume the likely formation of PbI_2 at grain boundaries, passivating $CH_3NH_3PbI_3$.[36–38] The series resistance R_S in contrast increases for the reference and decreases for the irradiated device.

2.3 Self-healing

The *in-situ* measurements of the perovskite solar cells were continued after the proton irradiation was terminated. Surprisingly, J_{SC} increases continuously with time for the irradiated devices, as shown in Fig. 2(a), green circles. Fig. 3 therefore summarizes the time dependence of J_{SC}, V_{OC}, FF and efficiency of the reference and the irradiated device (black diamonds and red circles). Here, $t - t_{irr} = 0$ s corresponds to the end of the irradiation experiment. The short circuit current significantly recovers by 3 % within 10 minutes, as compared to the reference device (Fig. 3(a)). At the same time V_{OC} and FF remain rather constant for both devices (Fig. 3(b) and (c)). Accordingly the efficiency recovers continuously on the irradiated device after termination of the irradiation

The change of J_{SC} is mainly due to a change in the concentration of localized defects. Hence, this result shows that the perovskite solar cells possess a self-healing capability that lowers the number of defects caused by proton irradiation. It is important to note that self-healing occurs at room temperature.

Elevated radioactivity, originating from created instable isotopes, unfortunately forced us to stop recording the self-healing behavior for longer times. Devices instead had to be stored in the radiation controlled environment. After declination of the radioactivity to an acceptable level. (after 10 days) we were able to measure the devices again under simulated AM1.5G illumination. The result is a superimposition of two effects: (i) continued degradation and (ii)

self-healing in case of the irradiated device. Fig. 4 summarizes the photovoltaic parameters of 3 irradiated and 3 reference devices.

In agreement with the proton induced degradation on Fig. 2, the J_{SC} is reduced by around 3 mA/cm^2 on the irradiated device. In fact, the internal quantum efficiency (IQE) is reduced over the entire spectrum (Fig. 4(e)). However additional effects, such as the creation of color centers in the glass substrate [39,40] have to be considered. As a result some light will be absorbed in the glass and consequently, the performance and quantum efficiency of the solar cell decreases. Fig. 4(f) therefore shows the transmission spectra of ITO coated glass substrates before (black curve) and after proton irradiation (blue and red curves). The coloring of the glass affects the transmission spectra in the spectral range between 300 and 800 nm. This shading effect is depicted by the hatched areas in Fig. 4. The created shading effect is in coincidence with the difference in IQE (Fig. 4 (f)). The reduced J_{SC} therefore is entirely caused by the glass coloring. This implies that the self-healing observed in Fig. 3 proceeds over a long period of time. In the end the number of localized defects caused by proton irradiation approaches zero.

As remark, optical glasses can be stabilized against radiation induced coloring for example by adding lanthanum or cerium. [39] Hence preparation of perovskite solar cells that do not degrade at all in J_{SC} upon proton irradiation seems feasible.

Furthermore Fig. 4 (c) depicts an significantly higher V_{OC} for the irradiated devices. With 0.96 V the V_{OC} in fact is around 10mV higher than on the freshly prepared device. In addition the FF, shown in Fig. 4(d), is around 15 % higher on the irradiated device.

Neglecting deleterious glass coloring, irradiated devices therefore should posess a power conversion efficiency exceeding 9 %. This is 25 % enhanced as compared to the reference device.

2.4 Discussion

Radiation induced damage is typically a consequence of a either elastic or inelastic scattering. In an elastic scattering process, a crystal atom is displaced to an interstitial position. Thus a Frenkel defect is created.[41] Inelastic scattering in contrast excites and ionizes via electronic interaction along the entire ion track. Secondary processes then may alter bond configurations, as e.g. described within the Coulomb-explosion model.[42,43]

The stopping power dE/dx of 68 MeV protons in $CH_3NH_3PbI_3$ may be approximated based on the Bragg rule using SRIM. [32] For elastic and inelastic scattering processes dE/dx amounts to 9.06×10^{-5} eV/Å and 0.25 eV/Å respectively. The dominating damage mechanism therefore is elastic scattering and the concomitant secondary processes.

In light of that, elastic scattering should also generate electron hole pairs. These will be separated in the build in field of the solar cell. Dedicated measurements allowed us to measure this generated current. The current exceeded 3 $\mu A/cm^2$. One incident proton therefore created over 1.1×10^5 electron hole pairs. The vast yield corroborates the fact that the observed defect creation is a consequence of the electronic excitation.

In particular, the energetic secondaries may break C-H, N-C or N-H bonds. The required energy is well below 4 eV. A fragmentation of methylammonium thus seems possible. Breaking of C-H bonds is well known upon irradiation of typical organic semiconductors such as P3HT[44] or PCDTBT[45]. Indeed Street et al. [45] proved that released hydrogen forms deep trap states acting as recombination centers in such organic semiconductors. It is likely that a similar mechanism creates the observed degradation in J_{SC}, via localized defects in $CH_3NH_3PbI_3$.

Recent combinations of theoretical calculations and EPR experiments proved the formation of localized defects well within the band gap for fragments of methylammonium.[46] Displaced

Pb and I atoms in contrary are expected to form shallow trap states only. [47,48] Experiments probing the localized state distribution should provide further insight.

Evidently the irradiation induced defect states are completely reversible. The mechanism of this self-healing is likely hydrogen migration and methylammonium reformation. The migration barrier of interstitial hydrogen in $CH_3NH_3PbI_3$ indeed is approximated to around 0.5 eV[49], and thus sufficient low. In order to provide some further insight we modelled the observed self-healing as thermally activated process. [45] The red line in Fig. 4(b) depicts a good fit to the model in equation (2).

$$\frac{J_{SC}(t)}{J_{SC}(t=0)} = C_0 + C_1 \cdot e^{-\frac{t}{\tau}} \; ; \; \tau = \omega_0^{-1} \cdot e^{\frac{E_A}{k_b T}} \qquad (2)$$

Hereby E_A denotes the activation energy and ω_0 the rate prefactor. Optimized parameters are $C_1 = 0.23$, $C_0 = 1.23$, and $\tau = 91$ min. Assuming a rate prefactor of $\omega_0 = 10^8$ min^{-1} yields an activation energy of $E_A = 0.6$ eV. As remark, further temperature dependent annealing experiments are needed to determine ω_0 and E_A accurately. However, changing the prefactor by an order of magnitude changes E_A by only 0.06 eV. The modelled data therefore suggest hydrogen migration as reason for the annealing of radiation induced trap states. On the other hand, low diffusion barriers around 0.6 eV are reported for iodine as well.[50] Therefore further experiments, clarifying the role of iodine or hydrogen migration on the self-healing of radiation induced defect states are needed.

The radiation hardness of $CH_3NH_3PbI_3$ in summary seems to be a consequence of the resilience to deep trap states. In detail, (i) interstitial iodine forms shallow defects only [47,48], while (ii) fragmentation of methylamine produces deep traps[46] with a high probability to self-heal even at room temperature.

3. Summary

In summary, we have fabricated inverted perovskite solar cells with a layer sequence of glass/ITO/PEDOT:PSS/$CH_3NH_3PbI_3$/PCBM/BCP/Ag. The inverted structure is beneficial for *in-situ* proton irradiation experiments since it does not suffer from a hysteresis effect in the $J - V$ characteristics. The solar cells had a stabilized power conversion efficiency of η = 12.1 %. The devices were irradiated with 68 MeV protons until a total dose of 1.02×10^{13} p cm^{-2} was reached. During the irradiation experiments *J*-V curves were measured every 30 s. A decrease of J_{SC} by 10 % and 60 % was observed for a proton dose of $\phi = 10^{12}$ p cm^{-2} and 10^{13} p cm^{-2}, respectively. However, when the data are corrected for deleterious effects, such as the photo degradation of the perovskite layer as measured on a reference, the decrease of J_{SC} amounts to only 3.8 % and 15.0 %. A degradation of V_{OC} is not observed. Hence, the perovskite absorber can withstand proton doses up to 10^{12} p cm^{-2}, which exceeds the damage threshold of c-Si by almost 3 orders of magnitude. Moreover, when the proton irradiation is terminated a self-healing process of the perovskite commences and J_{SC} recovers. A model explaining the completely reversible nature of the irradiation induced defects is discussed. After 10 days V_{OC} and FF were significantly enhanced, as compared to the reference device. The fact that $CH_3NH_3PbI_3$ perovskites are radiation hard and exhibit self-healing renders these solar cells highly attractive for space applications.

4. Experimental

Preparation of Perovskite Solar Cells: Planar inverted perovskite solar cells were prepared with the layer sequence glass/ITO/PEDOT:PSS/$CH_3NH_3PbI_3$/$PC_{61}BM$/BCP/Ag. First, the ITO coated glass substrates were cleaned using acetone, detergent/H_2O, H_2O, isopropanol, and O_3. Then, a 60 nm thick PEDOT:PSS (Heraeus PH 4083) layer was

deposited by spin-coating at 3000 rpm for 30 s. Subsequently, the PEDOT:PSS layer was annealed at 150 °C for 20 min.

A stoichiometric $CH_3NH_3PbI_3$ precursor solution containing 1.1 M of PbI_2 and CH_3NH_3I was prepared in a mixed solvent of γ-butryolactone and dimethyl sulfoxide with a volume ratio of 70 vol.% to 30 vol.%. The solution was stirred for 12 h at 60°C. In a second step, the $CH_3NH_3PbI_3$ solution was spin coated with the following sequence: 1000 rpm for 10 s, 2000 rpm for 20 s, and 5000 rpm for 20 s. At the last stage 150 µl toluene were dripped on top of the $CH_3NH_3PbI_3$ layer [28]. Spin coating was performed in nitrogen atmosphere. Subsequently, the $CH_3NH_3PbI_3$ layer was crystallized at 100 °C for 10 min. The absorber had a thickness of d = 350 nm. The electron selective contact was formed by spin coating a ~50 nm thick $PC_{61}BM$ layer at 2500 rpm for 60 s. After annealing for 10 min at 100 ºC a thin layer of bathocuproine (BCP) was spin coated from ethanol solution (0.5 mg/ml, 4000 rpm, 45 s). After annealing at 70°C for 15 min the devices were transferred into an evaporation chamber with a base pressure of about 10^{-7} mbar. Electrical contacts consisting of 100 nm Ag were thermally evaporated using a shadow mask. The overlap of the patterned ITO and the metal contacts defined the active area of the solar cells and amounted to 0.16 cm^2.

Characterization: The perovskite solar cells were characterized using an AM1.5G simulated solar spectrum provided by a 'Steuernagel Lichttechnik GmBH', or Newport LCS-100 class ABB sun simulator, both calibrated using an ISE certified Si reference solar cell. Because of the well-known hysteresis effect [25,27] current-voltage scans were performed in forward and reverse direction using a voltage sweep of 85 mV/s. For the inverted solar cell structures, a hysteresis was not observed and the maximum power points for forward and reverse scan directions were identical. The external quantum efficiency was measured without bias voltage and illumination. Prior to characterization perovskite solar cells were light soaked for 30 min. The proton irradiation experiments were performed at the cyclotron of the

Helmholtz-Zentrum Berlin. [33,34] The proton energy was 68 MeV. The Tandetron-cyclotron combination provides a high stability of the beam intensity. To achieve a homogeneous irradiation over an area of 3.0 cm^2 wobbler magnets were used. The beam intensity was monitored online using a transmission ionization chamber from 'PTW Freiburg GmbH'. During proton irradiation *in-situ* measurements were performed using a halogen lamp. The light intensity was about 25 mW/cm^2 A crystalline silicon photo-diode 'BPW34' purchased from Vishay semiconductors was used as reference.

Acknowledgements

The authors are grateful to C. Klimm for taking SEM micrographs. Financial support from the Helmholtz Energy Alliance (Hybrid Photovoltaic) and the Seventh Framework Program of the European Union under grant No. 604032 is acknowledged. V. V. Brus acknowledges the Alexander-von-Humboldt foundation for financial support.

Figures

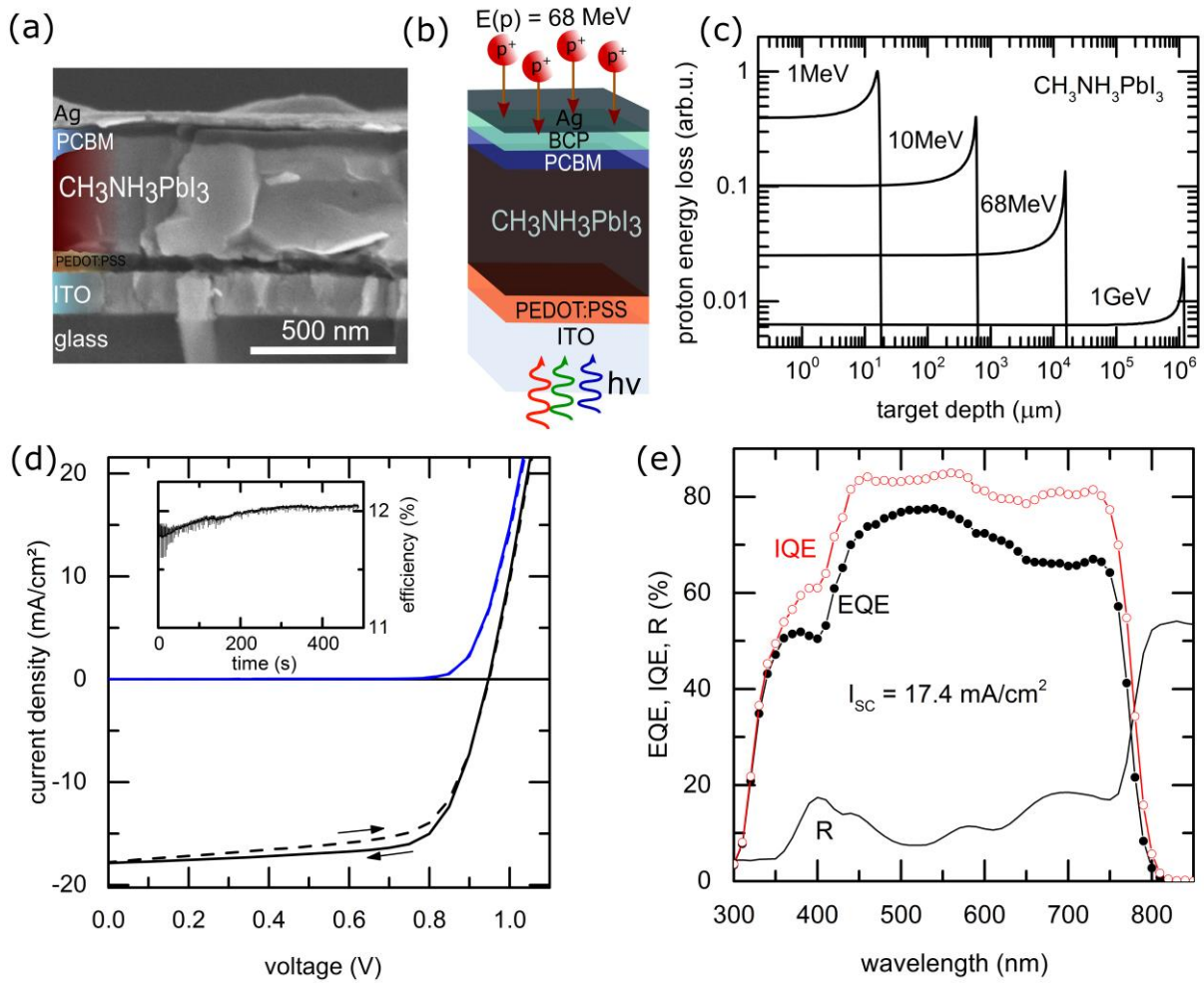

Fig. 1. (a) Cross-sectional SEM micrograph of an inverted perovskite solar cell consisting of the layer stack glass/ITO/PEDOT:PSS/$CH_3NH_3PbI_3$/PCBM/BCP/Ag. A sketch of the perovskite solar cell is depicted in (b). Proton irradiation was performed through the Ag electrode while the device was illuminated through the glass substrate. (c) Projected range of the proton beam in the perovskite $CH_3NH_3PbI_3$. The simulation was performed using SRIM [32]. Current-voltage characteristics of the perovskite solar cell before irradiation, taken in the dark (blue curve) and under AM1.5G illumination (black curve) are shown in (d). The scan direction of the voltage is indicated by arrows. A hysteresis between reverse scan (solid lines) and forward scan (dashed lines) is negligible. The inset shows the stabilized efficiency from maximum power point tracking. (e) Shows the external (EQE) and internal (IQE) quantum efficiencies. The black solid line depicts the specular reflection.

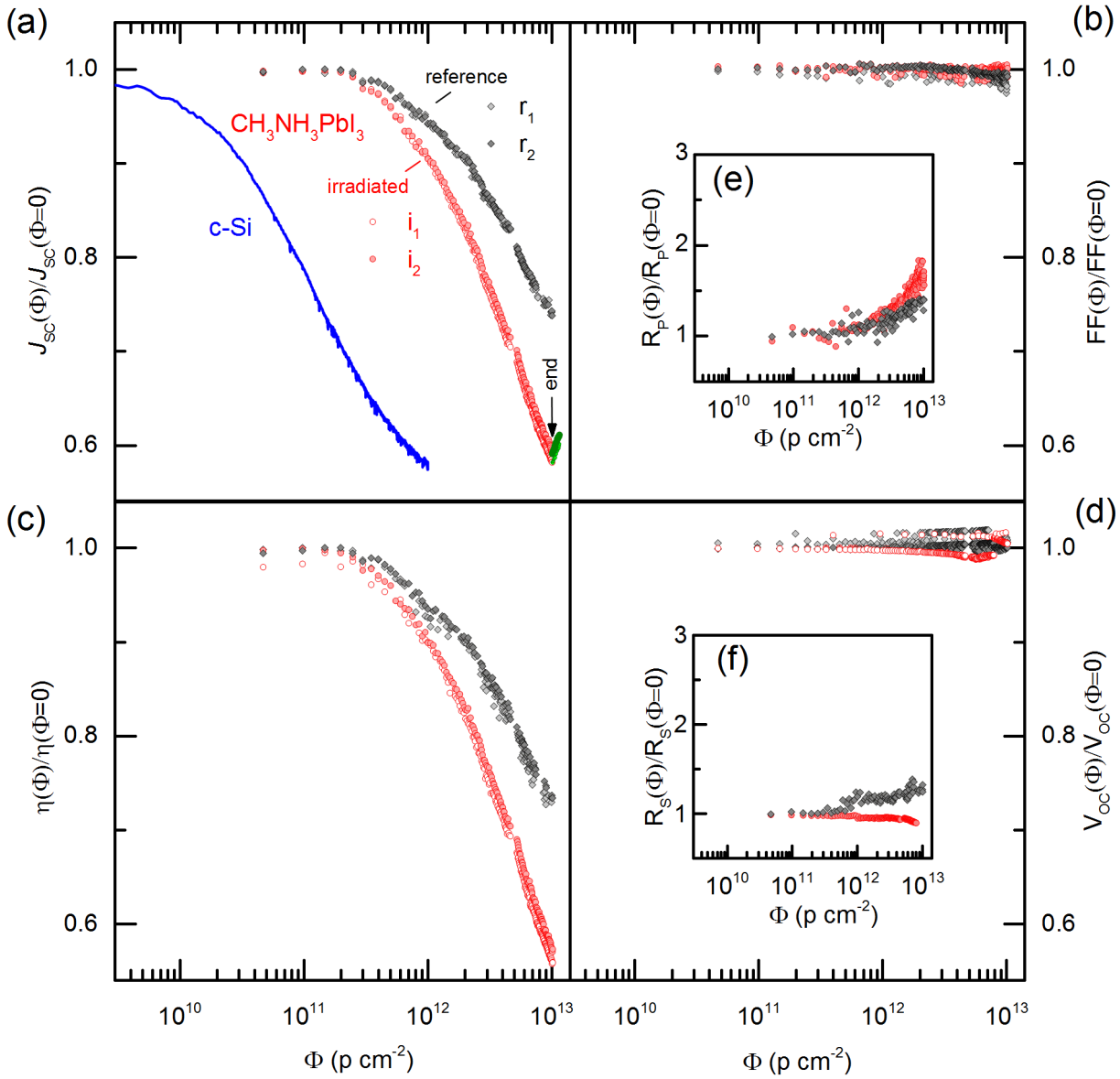

Fig. 2. Normalized solar cell parameters as a function of the proton dose, ϕ, for two perovskite solar cells (red filled and open circles) and a c-Si photo-diode (blue curve). Black open and closed symbols show data of two simultaneously measured perovskite solar cells without proton exposure, serving as reference. In detail figure (a), (b), (c) and (d) show the evolution of the short circuit current *J*sc, the fill factor FF, the efficiency η and the open circuit voltage V_{OC}. The insets (e) and (f) show the evolution of the derived parallel R_P and series resistance R_S.

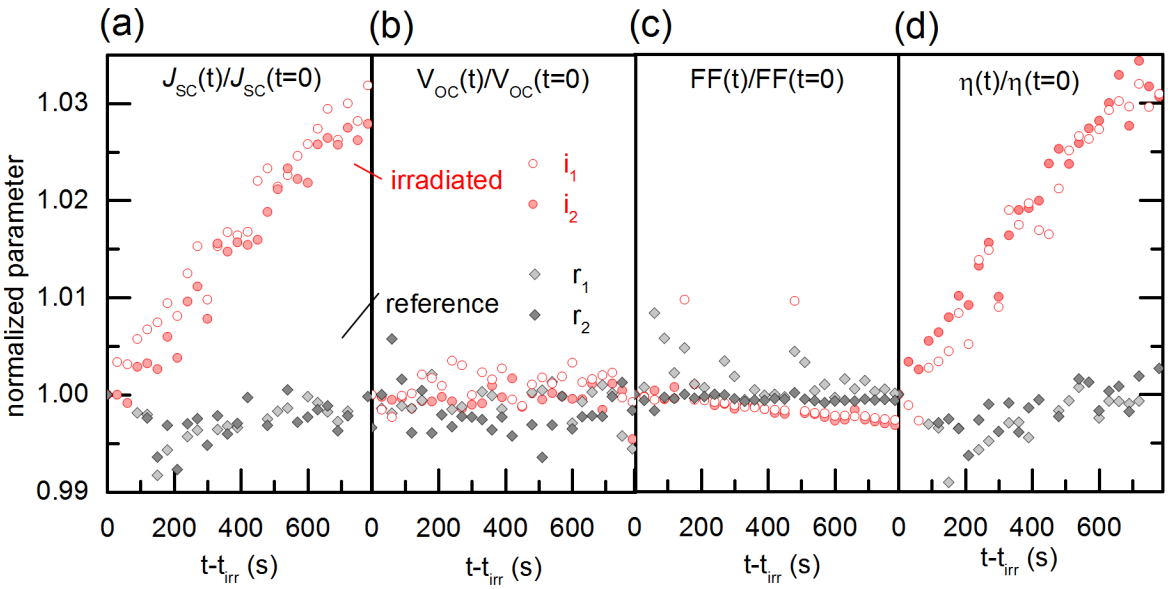

Fig. 3. Time dependence of the normalized solar cell parameters after termination of the proton irradiation for two irradiated devices (red filled and open circles) and two reference devices (black open and closed diamonds). The data is normalized to unity at t=0.

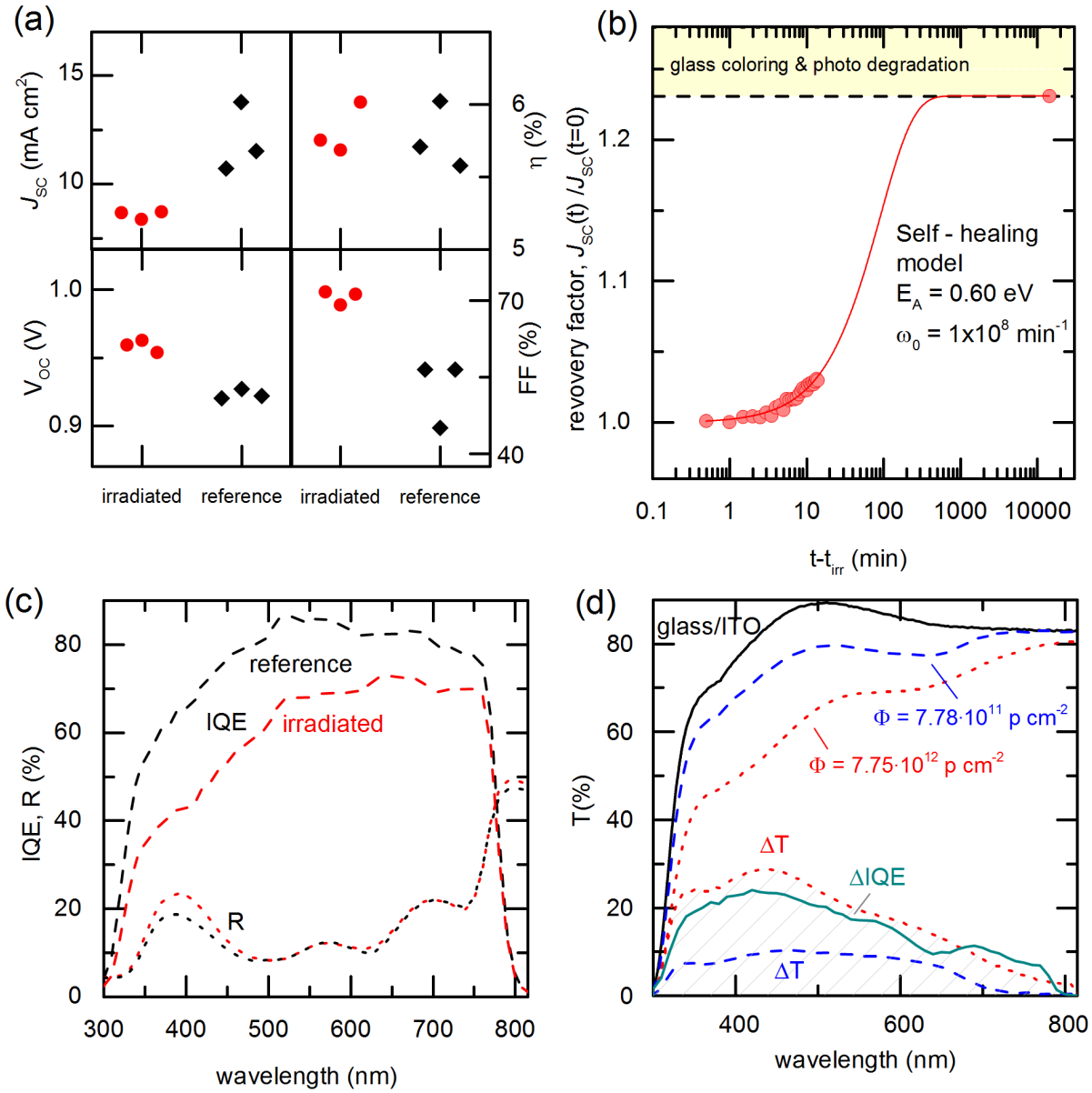

Fig. 4. (a) Depicts a detailed comparison of the photovoltaic parameters J_{SC}, V_{OC}, η and FF under AM1.5G, taken after the radioactivity dropped to a bearable level (after 10 days). (b) Recovery of the J_{SC} and optimized self-healing model, as described in the text (e) Internal quantum efficiency (IQE) and reflection (R) of the reference (black) and the irradiated device (red, ϕ =10^{13} p cm^{-2}). (f) Diffuse transmission of glass/ITO substrates before (black solid curve) and after proton irradiation with a dose of ϕ = 7.78×10^{11} p cm^{-2} (blue dashed curve) and ϕ = 7.75×10^{12} p cm^{-2} (red dotted line). The resulting shading (ΔT) is shown by hatched red and blue curves. The difference in the internal quantum efficiencies (ΔIQE) from (e) is plotted as solid grey line.

Reference:

[1] W. S. Yang, J. H. Noh, N. J. Jeon, Y. C. Kim, S. Ryu, J. Seo, S. I. Seok, *Science* **2015**, *348*, 1234.

[2] H. J. Snaith, *J. Phys. Chem. Lett.* **2013**, *4*, 3623.

[3] J. H. Noh, S. H. Im, J. H. Heo, T. N. Mandal, S. Il Seok, *Nano Lett.* **2013**, *13*, 1764.

[4] M. R. Filip, G. E. Eperon, H. J. Snaith, F. Giustino, *Nat. Commun.* **2014**, *5*, 5757.

[5] D. P. McMeekin, G. Sadoughi, W. Rehman, G. E. Eperon, M. Saliba, M. T. Horantner, A. Haghighirad, N. Sakai, L. Korte, B. Rech, M. B. Johnston, L. M. Herz, H. J. Snaith, *Science* **2016**, *351*, 151.

[6] F. Lang, M. A. Gluba, S. Albrecht, J. Rappich, L. Korte, B. Rech, N. H. Nickel, *J. Phys. Chem. Lett.* **2015**, *6*, 2745.

[7] S. Albrecht, M. Saliba, J. P. Correa Baena, F. Lang, L. Kegelmann, M. Mews, L. Steier, A. Abate, J. Rappich, L. Korte, R. Schlatmann, M. K. Nazeeruddin, A. Hagfeldt, M. Grätzel, B. Rech, *Energy Environ. Sci.* **2016**, *9*, 81.

[8] P. Löper, S.-J. Moon, S. Martín de Nicolas, B. Niesen, M. Ledinsky, S. Nicolay, J. Bailat, J.-H. Yum, S. De Wolf, C. Ballif, *Phys. Chem. Chem. Phys.* **2015**, *17*, 1619.

[9] L. Kranz, A. Abate, T. Feurer, F. Fu, E. Avancini, J. Löckinger, P. Reinhard, S. M. Zakeeruddin, M. Grätzel, S. Buecheler, A. N. Tiwari, *J. Phys. Chem. Lett.* **2015**, *6*, 2676.

[10] R. Sheng, A. W. Y. Ho-Baillie, S. Huang, M. Keevers, X. Hao, L. Jiang, Y.-B. Cheng, M. A. Green, *J. Phys. Chem. Lett.* **2015**, *6*, 3931.

[11] J. Werner, G. Dubuis, A. Walter, P. Löper, S.-J. Moon, S. Nicolay, M. Morales-Masis, S. De Wolf, B. Niesen, C. Ballif, *Sol. Energy Mater. Sol. Cells* **2015**, *141*, 407.

[12] F. Fu, T. Feurer, T. Jäger, E. Avancini, B. Bissig, S. Yoon, S. Buecheler, A. N. Tiwari, *Nat. Commun.* **2015**, *6*, 8932.

[13] C. D. Bailie, M. G. Christoforo, J. P. Mailoa, A. R. Bowring, E. L. Unger, W. H. Nguyen, J. Burschka, N. Pellet, J. Z. Lee, M. Grätzel, R. Noufi, T. Buonassisi, A. Salleo, M. D. McGehee, *Energy Environ. Sci.* **2014**, *8*, 956.

[14] T. Todorov, T. Gershon, O. Gunawan, Y. S. Lee, C. Sturdevant, L.-Y. Chang, S. Guha, *Adv. Energy Mater.* **2015**, *5*, 1500799.

[15] B. Todd, S. Uznanski, *CAS - Cern Accel. Sch. Power Convert.* **2015**, *003*, 1.

[16] R. Schwenn, In *The Encyclopedia of Astronomy and Astrophysics*; IOP Publishing Ltd, 2001; pp. 1–9.

[17] D. Mottl, R. Nymmik, *Adv. Space Res.* **2003**, *32*, 2349.

[18] T. Markvart, *J. Mater. Sci. Mater. Electron.* **1990**, *1*, 1.

[19] E. J. Daly, G. Drolshagen, A. Hilgers, H. D. R. Evans, *Space Environment Analysis: Experience and Trends*.

[20] A. Jasenek, U. Rau, K. Weinert, H. W. Schock, J. H. Werner, *Photovolt. Energy Conversion, 2003. Proc. 3rd World Conf.* **2003**, *1*, 593.

[21] S. R. Messenger, G. P. Summers, E. A. Burke, R. J. Walters, M. A. Xapsos, *Prog. Photovoltaics Res. Appl.* **2001**, *9*, 103.

[22] P. Iles, *Sol. Energy Mater. Sol. Cells* **2001**, *68*, 1.

[23] A. Kumar, R. Devine, C. Mayberry, B. Lei, G. Li, Yang, *Adv. Funct. Mater*. **2010**, *20*, 2729.

[24] X. Zhao, N.-G. Park, *Photonics* **2015**, *2*, 1139.

[25] H. J. Snaith, A. Abate, J. M. Ball, G. E. Eperon, T. Leijtens, N. K. Noel, S. D. Stranks, J. T.-W. Wang, K. Wojciechowski, W. Zhang, *J. Phys. Chem. Lett.* **2014**, *5*, 1511.

[26] H.-S. Kim, I.-H. Jang, N. Ahn, M. Choi, A. Guerrero, J. Bisquert, N.-G. Park, *J. Phys. Chem. Lett.* **2015**, *6*, 4633.

[27] E. L. Unger, E. T. Hoke, C. D. Bailie, W. H. Nguyen, A. R. Bowring, T. Heumuller, M. G. Christoforo, M. D. McGehee, *Energy Environ. Sci.* **2014**, *7*, 3690.

[28] N. J. Jeon, J. H. Noh, Y. C. Kim, W. S. Yang, S. Ryu, S. Il Seok, *Nat. Mater.* **2014**, *13*, 897.

[29] G. D. Badhwar, P. M. O'Neill, *Int. J. Radiat. Appl. Instrumentation. Part D. Nucl. Tracks Radiat. Meas.* **1992**, *20*, 403.

[30] G. D. Badhwar, P. M. O'Neill, *Adv. Space Res.* **1996**, *17*, 7.

[31] H. C. Neitzert, P. Spinillo, S. Bellone, G. D. Licciardi, M. Tucci, F. Roca, L. Gialanella, M. Romano, *Sol. Energy Mater. Sol. Cells* **2004**, *83*, 435.

[32] J. F. Ziegler, M. D. Ziegler, J. P. Biersack, *Nucl. Instruments Methods Phys. Res. Sect. B Beam Interact. with Mater. Atoms* **2010**, *268*, 1818.

[33] A. Denker, C. Rethfeldt, J. Röhrich, H. Berlin, D. Cordini, J. Heufelder, R. Stark, A. Weber, B. H. Berlin, *Proc. CYCLOTRONS 2010, (Lanzhou, China)* **2010**, 75.

[34] J. Röhrich, T. Damerow, W. Hahn, U. Müller, U. Reinholz, A. Denker, *Rev. Sci. Instrum.* **2012**, *83*, 02B903.

[35] H.-C. Neitzert, M. Ferrara, M. Kunst, A. Denker, Z. Kertész, B. Limata, L. Gialanella, M. Romano, *Phys. status solidi B* **2008**, *245*, 1877.

[36] V. Somsongkul, F. Lang, A. R. Jeong, M. Rusu, M. Arunchaiya, T. Dittrich, *Phys. status solidi - Rapid Res. Lett.* **2014**, *08*, 763.

[37] Q. Chen, H. Zhou, T.-B. Song, S. Luo, Z. Hong, H.-S. Duan, L. Dou, Y. Liu, Y. Yang, *Nano Lett.* **2014**.

[38] T. Supasai, N. Rujisamphan, K. Ullrich, A. Chemseddine, T. Dittrich, *Appl. Phys. Lett.* **2013**, *103*, 183906.

[39] A. I. Gusarov, D. Doyle, A. Hermanne, F. Berghmans, M. Fruit, G. Ulbrich, M. Blondel, *Appl. Opt.* **2002**, *41*, 678.

[40] M. F. Bartusiak, J. Becher, *Appl. Opt.* **1979**, *18*, 3342.

[41] J. J. Loferski, P. Rappaport, *Phys. Rev.* **1958**, *111*, 432.

[42] G. Schiwietz, K. Czerski, M. Roth, F. Staufenbiel, P. L. Grande, *Nucl. Instruments*

Methods Phys. Res. Sect. B Beam Interact. with Mater. Atoms **2004**, *226*, 683.

[43] E. M. Bringa, R. E. Johnson, *Phys. Rev. Lett.* **2002**, *88*, 165501.

[44] F. Bebensee, J. Zhu, J. H. Baricuatro, J. A. Farmer, Y. Bai, H. P. Steinrück, C. T. Campbell, J. M. Gottfried, *Langmuir* **2010**, *26*, 9632.

[45] R. A. Street, J. E. Northrup, B. S. Krusor, *Phys. Rev. B - Condens. Matter Mater. Phys.* **2012**, *85*, 1.

[46] P. Delugas, A. Filippetti, A. Mattoni, *Phys. Rev. B - Condens. Matter Mater. Phys.* **2015**, *92*, 1.

[47] W.-J. Yin, T. Shi, Y. Yan, *Appl. Phys. Lett.* **2014**, *104*, 063903.

[48] J. Kim, S. H. Lee, J. H. Lee, K. H. Hong, *J. Phys. Chem. Lett.* **2014**, *5*, 1312.

[49] D. A. Egger, L. Kronik, A. M. Rappe, *Angew. Chemie Int. Ed.* **2015**, *54*, 12437.

[50] C. Eames, J. M. Frost, P. R. F. Barnes, B. C. O'Regan, A. Walsh, M. S. Islam, *Nat. Commun.* **2015**, *6*, 7497.

The radiation hardness of $CH_3NH_3PbI_3$ based solar cells is evaluated from *in-situ* measurements during high-energy proton irradiation. These organic-inorganic perovskites exhibit radiation hardness and withstand proton doses that exceed the damage threshold of c-Si by almost 3 orders of magnitude. Moreover, after termination of the proton irradiation a self-healing process of the solar cells commences. Radiation hardness and self-healing renders these solar cells highly attractive for space applications.

ToC figure: